Robots' Motion Planning in Human Crowds by Acceleration Obstacles

David J. Gonon, Diego Paez-Granados, and Aude Billard, *Fellow, IEEE*

***Abstract*—We study the Acceleration Obstacle (AO) as a concept to enable a robot's navigation in human crowds. The AO's geometric properties are analyzed and a direct sampling-free algorithm is proposed to approximate its boundary by linear constraints. The resulting controller is formulated as a quadratic program and evaluated in interaction with simulated bi-directional crowd flow in a corridor. We compare it to alternative robotic controllers, considering the robot's and the crowd's performance and the robot's behavior with respect to emergent lanes. Our results indicate that the robot can achieve higher efficiency when being less integrated in lanes.**

***Index Terms*—Automation technologies for smart cities, human-aware motion planning, path planning for multiple mobile robots or agents.**

I. Introduction

ROBOTS that navigate in human crowds as seamlessly as pedestrians are a persistent goal of recent work in robotics due to applications as delivery robots or smart wheelchairs. Some works [1], [2] focus on predicting pedestrians' motion in the near future, which allows to choose a complementary action for a robot amidst them. Other methods [3], [4] model the crowd's uncertain behavior to find motions for the robot that are safe under worst case assumptions. Geometric approaches, such as the Velocity Obstacle (VO) [5], [6], allow to command the robot such that it avoids collisions with obstacles whose motion is known in the near future. In this letter, we investigate the Acceleration Obstacle (AO) in analogy to VO, assuming that the robot and obstacles maintain constant relative acceleration (instead of velocity as for VO) over a short time span. Our choice to assume constant acceleration is motivated by the mathematical simplicity of this motion model, which facilitates our analysis of AO.

The AO for a given obstacle defines a set of relative accelerations whose constant application will lead to a collision before reaching a time horizon. In comparison to the VO, whose shape can be described as a cone with a round truncated tip, the AO exhibits a more complex shape, whose entire boundary is curved in general. Similar shapes have been defined in prior work [7], [8], where typically, the boundary is approximated by a linear constraint, which is imposed on the robot's command. However, the boundary's geometric properties and dependence on initial conditions (i.e. the relative position and velocity for AO) has not been studied in depth in prior work. Our analysis reveals how the geometric properties of AO emerge (Section II). Exploiting this analysis, a novel algorithm is proposed which derives a linear approximation of the AO via a few geometric and algebraic computations in closed form (Section III).

Previous work [7] has conceived the AO without studying it further, arguing that constant accelerations are rarely maintained over extended time spans, and proposing instead the related concept of the Acceleration Velocity Obstacle (AVO), which assumes exponential adoption of a target velocity. However, our experiments of navigation in human crowds show that a small time horizon is sufficient to avoid collisions under realistic acceleration capabilities. As an advantage over AVO, the AO requires the smallest peak deceleration for braking in front of an obstacle, which we illustrate in simulation. We also show that the AO can be expressed via the AVO and a limit operation. Therefore, the theory and algorithm presented in this letter appear to generalize to AVO.

Acceleration bounds are also considered by another geometric approach termed as the forbidden velocity map [9], which specifies for any given direction the largest speed which still allows the robot to brake before a collision occurs. The AO is a more general approach as its motion model includes curved trajectories and thus allows to plan maneuvers which apply maximum acceleration to avoid collisions by passing at the side of an obstacle rather than braking in front of it.

The experimental evaluation in this letter focuses on navigation in bi-directional crowd flow through a corridor. We show that the AO with the proposed algorithm enables the robot to navigate efficiently and avoid almost all collisions, outperforming pedestrians, which are simulated by the Social Force Model (SFM) [10]. As a baseline, we use the SFM to control the robot like a pedestrian. Since both the AO and the SFM refer to accelerations, one can combine them, which is explored as one alternative method for comparison.

We also study the robot's behavior with respect to emergent lanes in the crowd's motion. Lanes lead to more efficient motions [11] and have been shown to emerge under a variety of

Manuscript received 7 March 2022; accepted 26 July 2022. Date of publication 18 August 2022; date of current version 29 August 2022. This letter was recommended for publication by Associate Editor M. Rajesh Elara and Editor G. Venture upon evaluation of the reviewers' comments. This work was supported in part by the EU H2020 project "Crowdbot" under Grant 779942 and in part by Hasler Foundation, Switzerland. *(Corresponding author: David J. Gonon.)*

David J. Gonon and Aude Billard are with the School of Engineering, EPFL, 1015 Lausanne, Switzerland (e-mail: david.gonon@epfl.ch; aude.billard@epfl.ch).

Diego Paez-Granados is with the Spinal Cord Injury Artificial Intelligence - SCAI - Lab at SPZ, ETH Zurich, 8092 Zürich, Switzerland (e-mail: dfpg@ieee.org).

This letter has supplementary downloadable material available at https://doi.org/10.1109/LRA.2022.3199818, provided by the authors.

Digital Object Identifier 10.1109/LRA.2022.3199818

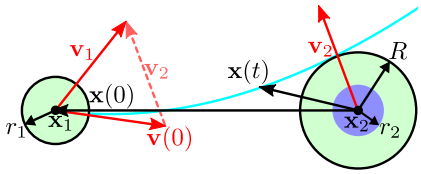

Fig. 1. The state of the robot and the obstacle with the respective positions $\mathbf{x}_1$, $\mathbf{x}_2$ and velocities $\mathbf{v}_1$, $\mathbf{v}_2$ is represented for AO by the relative position $\mathbf{x}$ and velocity $\mathbf{v}$ and the collider with the combined radius $R = r_1 + r_2$. A motion (cyan) over time t with constant acceleration of $\mathbf{x}(t)$ is shown.

interaction laws, including the SFM [10], [11] and the reciprocal VO [6], [12], which implements local pairwise collision avoidance. However, a robot's interaction with emergent patterns (such as lanes) arising in a crowd of agents whose characterstics differ from the robot, has rarely been evaluated, to the best of our knowledge. We systematically evaluate how the robot's method for navigation affects its own and the crowd's performance (Section IV). Specifically, we count collisions and near misses between the robot and the crowd and quantify the robot's and the crowd's efficiency of motion in terms of velocity and path length. Additionally, we measure the robot's integration in lanes and its interaction intensity with the counter flow.

Notation: Let $\mathbf{p} \times \mathbf{q} := p_1 q_2 - p_2 q_1$ denote the cross product for vectors $\mathbf{p}, \mathbf{q} \in \mathbb{R}^2$. For a set $G \subset \mathbb{R}^2$, let $\partial G \subset \mathbb{R}^2$ denote its boundary and $|G|$ its cardinality. Let $D(\mathbf{p}, \varrho) := \{\mathbf{z} \,|\, \varrho \geq |\mathbf{z} - \mathbf{p}|^2\} \subset \mathbb{R}^2$ denote the closed disk with radius ϱ centered on $\mathbf{p}$. We use $\dot{\mathbf{x}} := \mathrm{d}\mathbf{x}/\mathrm{d}t$.

II. Acceleration Obstacles

For a mobile robot and an obstacle (cf. Fig. 1) with the respective positions $\mathbf{x}_1, \mathbf{x}_2 \in \mathbb{R}^2$, we consider the task of collision-free navigation. Let $\mathbf{x} := \mathbf{x}_1 - \mathbf{x}_2$ define the relative position. The two agents' bodies' shapes are bounded by two circles whose radii are given by r_1, r_2, and whose centers are at $\mathbf{x}_1$, $\mathbf{x}_2$, respectively. With the combined radius $R := r_1 + r_2$, a collision is said to occur if $|\mathbf{x}| \leq R$.

For defining the AO, we consider the motion model of constant relative acceleration $\mathbf{a} = const$. The family of relative trajectories satisfying $\ddot{\mathbf{x}} = \mathbf{a}$ is given by

$$\mathbf{x}(t; \mathbf{a}) := \mathbf{x}_o + \mathbf{v}_o t + \mathbf{a}t^2/2 \tag{1}$$

with the parameter $\mathbf{a}$, for given initial conditions $\mathbf{x}(0) = \mathbf{x}_o$ and $\dot{\mathbf{x}}(0) = \mathbf{v}_o$. The model $\ddot{\mathbf{x}} = const$ can represent two agents applying constant forces (to avoid each other) and thereby approximate pedestrians' behavior over a short time window. The AO is the set of accelerations $\mathbf{a}$ that lead to a collision before a time horizon τ. It is formalized as follows.

Definition 1 (Acceleration Obstacle): The Acceleration Obstacle with the time horizon τ for the robot and a given obstacle with the relative position and velocity $\mathbf{x}_o$ and $\mathbf{v}_o$, respectively, and the combined radius R is the set

$$AO_\tau(\mathbf{x}_o, \mathbf{v}_o, R) := \{\mathbf{a} \,|\, \exists t \in [0, \tau] : |\mathbf{x}(t; \mathbf{a})| \leq R\}. \tag{2}$$

We note that $|\mathbf{x}(t; \mathbf{a})| \leq R \iff \mathbf{a} \in D(\mathbf{c}(t), r(t))$ with

$$\mathbf{c}(t) := -2\left(\mathbf{x}_o + t\mathbf{v}_o\right)/t^2, \quad r(t) := 2R/t^2, \tag{3}$$

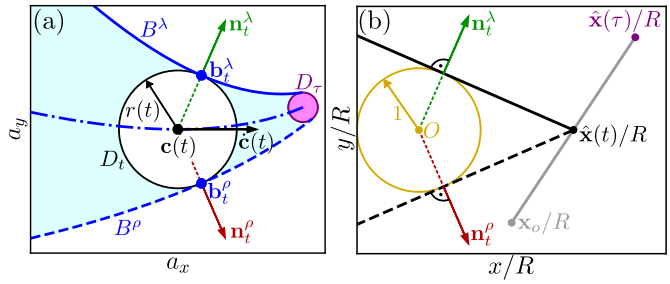

Fig. 2. (a) Showing an AO_τ, its sweeping disk D_t with center $\mathbf{c}(t)$ and radius $r(t)$ for some time $t \in (0, \tau]$, the local boundary's elements $\mathbf{b}_t^\lambda$ and $\mathbf{b}_t^\rho$, which are left and right with respect to the center's derivative $\dot{\mathbf{c}}(t)$, and their unions B^λ and B^ρ, respectively, up to the time horizon's disk D_τ. (b) Showing the (normalized) extrapolation $\hat{\mathbf{x}}(t)/R$ from $\mathbf{x}_o/R$ over $[0, \tau]$ in the space of the normalized relative position coordinates x/R and y/R. The unit circle's tangents through $\hat{\mathbf{x}}(t)/R$ are orthogonal to the AO_τ's local normals $\mathbf{n}_t^\lambda$ and $\mathbf{n}_t^\rho$ at any given time $t \in (0, \tau]$ with $|\hat{\mathbf{x}}(t)| > R$.

due to (1). Thus, we express the AO_τ given by (2) as

$$\begin{aligned} AO_\tau &= \{\mathbf{a} \,|\, \exists t \in (0, \tau] : \mathbf{a} \in D(\mathbf{c}(t), r(t))\} \\ &= \bigcup_{t \in (0,\tau]} D(\mathbf{c}(t), r(t)) = \bigcup_{t \in (0,\tau]} D_t \end{aligned} \tag{4}$$

with $D_t := D(\mathbf{c}(t), r(t))$. The final expression (4) describes the AO as a union of disks defined over the time span $(0, \tau]$ (cf. Fig. 2(a)), i.e. a planar shape analogous to a *canal* (i.e. a union of spheres) in $\mathbb{R}^3$ [13]. The last disk's boundary $\partial D_\tau \cap \partial AO_\tau$ is associated with collisions at the time horizon, whereas the remaining boundary corresponds to grazing motions. It is generally curved, since the acceleration term in (1) is combined with the growing translation $t\mathbf{v}_o$, such that $\mathbf{a}$ must rotate to reach the collider at different times.

A. Geometric Properties of Acceleration Obstacles

For discussing the shape of the AO, we first define precise notions of its boundary and normals (cf. also Fig. 2).

Definition 2 (Local Boundary/Normals): For an AO_τ, the local boundary at $t \in (0, \tau]$ is the set

$$B_t := \lim_{\Delta t \to 0} \partial D_t \cap \partial D_{t+\Delta t}. \tag{5}$$

The set of (outwards) normals at $t \in (0, \tau]$ is defined as

$$N_t := \{\mathbf{u} \,|\, \mathbf{u} = (\mathbf{b}_t - \mathbf{c}(t))/r(t), \mathbf{b}_t \in B_t\}. \tag{6}$$

Thus, we associate with any given element $\mathbf{b}_t \in B_t$ a normal $\mathbf{n}_t \in N_t$. If $|N_t| = 2$, the two normals are denoted by $\mathbf{n}_t^\lambda$ and $\mathbf{n}_t^\rho$, such that $\dot{\mathbf{c}} \times \mathbf{n}_t^\lambda > 0$ and $\dot{\mathbf{c}} \times \mathbf{n}_t^\rho < 0$, and termed as *left* and *right* (relative to $\dot{\mathbf{c}}$), respectively. Their corresponding boundary points are denoted by $\mathbf{b}_t^\lambda$, $\mathbf{b}_t^\rho$, accordingly.

The normals N_t can be constructed via the *extrapolation* $\hat{\mathbf{x}}(t) := \mathbf{x}_o + \mathbf{v}_o t/2$ according to the following proposition (cf. Fig. 2), which is proven in the Appendix A.

Proposition 1 (AO-normals): For the $AO_\tau(\mathbf{x}_o, \mathbf{v}_o, R)$, the set of normals at any $t \in (0, \tau]$ is given by

$$N_t = \left\{\mathbf{u} \middle| \mathbf{u}^T \hat{\mathbf{x}}(t) - R = 0, |\mathbf{u}| = 1\right\}. \tag{7}$$

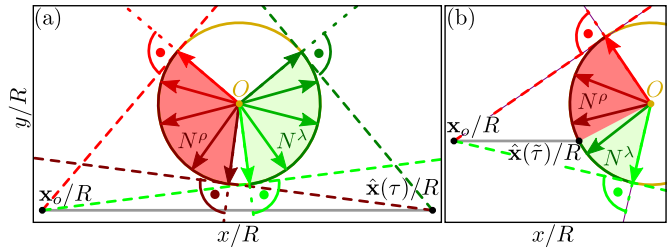

Fig. 3. The tangents through the (normalized) extrapolation $\hat{\mathbf{x}}(t)/R$ touch the unit circle at the respective AO_τ's normals. Thereby, the left and right normals' unions N^λ and N^ρ are generated, respectively, as t varies over $(0, \tilde{\tau})$. The reduced time horizon $\tilde{\tau}$ can be (a) equal to the time horizon τ or (b) smaller than τ (if the line from $\mathbf{x}_o$ to $\hat{\mathbf{x}}(\tau)$ intersects the unit circle).

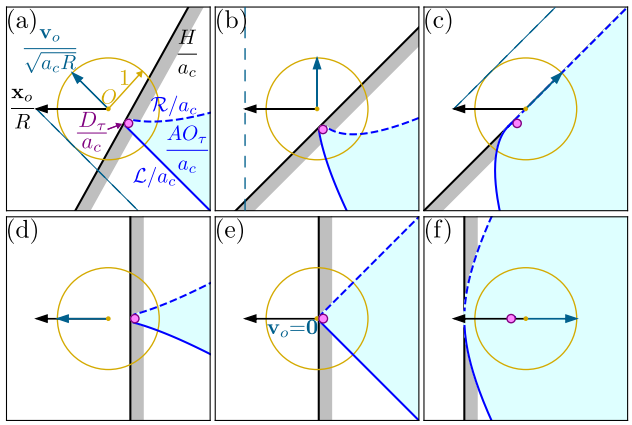

Fig. 4. Each plot (a-f) shows an AO_τ, its left and right boundaries $\mathcal{L}$ and $\mathcal{R}$, respectively, the underlying relative initial position $\mathbf{x}_o$ (fixed) and velocity $\mathbf{v}_o$ (varying), the final disk D_τ, and the halfplane H by the Algorithm 1, normalized via the combined radius R and the unit acceleration a_c. The initial course is post-colliding (d), left-passing (b), and pre-colliding (f), or an edge case, if the dashed line through $\mathbf{x}_o/R$ and parallel to $\mathbf{v}_o$ touches the unit circle (a, c) or $\mathbf{v}_o = 0$ (e).

Thus, the normals are constructed from tangents to the unit circle (i.e. the normalized collider) through the normalized extrapolation $\hat{\mathbf{x}}(t)/R$ as the Fig. 2(b) illustrates. One can also use $\hat{\mathbf{x}}$ instead of $\dot{\mathbf{c}}$ as reference to identify which is the left or right normal, since $\dot{\mathbf{c}}(t) = 4\hat{\mathbf{x}}(t)/t^3$ holds, as can be derived from (3), i.e. the two references differ only by scaling.

Since $|B_t| = |N_t|$, the local boundary exists at a given t if (7) admits any solutions, which is the case iff $|\hat{\mathbf{x}}(t)| \geq R$. Thus, assuming that the initial state is not in collision, the AO_τ's local boundary exists from time zero up to the *reduced time horizon* $\tilde{\tau}$ defined as (cf. Fig. 3(b))

$$\tilde{\tau} := \max\left\{t | \forall t' < t : |\hat{\mathbf{x}}\left(t'\right)| > R, t \leq \tau\right\}. \tag{8}$$

Further, $\tilde{\tau}$ is sufficient as a horizon, in the sense of the following proposition, which is proven in the Appendix B.

Proposition 2 (AO-reduction): The interval $(0, \tilde{\tau}]$ already generates the complete AO_τ, i.e. $AO_{\tilde{\tau}} = AO_\tau$.

Accordingly, we define the *left local boundary's union* $B^\lambda := \{\mathbf{z} | \mathbf{z} = \mathbf{b}_t^\lambda, t \in (0, \tilde{\tau})\}$ and the *left normals' union* $N^\lambda := \{\mathbf{u} | \mathbf{u} = \mathbf{n}_t^\lambda, t \in (0, \tilde{\tau})\}$, uniting elements up to $\tilde{\tau}$. The *right local boundary's union* B^ρ and the *right normals' union* N^ρ are defined analogously. The Figs. 2 and 3 illustrate respectively the local boundaries' and normals' unions.

We partition the AO_τ's boundary ∂AO_τ into the *left boundary* $\mathcal{L} \subseteq B^\lambda$, the *right boundary* $\mathcal{R} \subseteq B^\rho$, and the *cap* $\mathcal{C} \subset \partial D_{\tilde{\tau}}$, where $\mathcal{C}$ contains at least a single point and connects $\mathcal{L}$ and $\mathcal{R}$. As B^λ or B^ρ can form a self-intersecting curve, a point on B^λ or B^ρ does not necessarily belong to the AO_τ's actual boundary ∂AO_τ.

The Proposition 3 below characterizes the AO_τ's local convexity or concavity on its boundary's partitions $\mathcal{L}$ and $\mathcal{R}$ dependent on the following definition's terminology.

Definition 3 (Initial Course): The initial course defined by the tuple $(\mathbf{x}_o, \mathbf{v}_o, R)$ is termed as

- *pre-colliding* if $\exists t > 0 : |\hat{\mathbf{x}}(t)| < R$
- *post-colliding* if $\exists t < 0 : |\hat{\mathbf{x}}(t)| < R$
- *left-passing* if $\forall t : \mathbf{v}_o \times \hat{\mathbf{x}}(t) > 0 \wedge |\hat{\mathbf{x}}(t)| > R$
- *right-passing* if $\forall t : \mathbf{v}_o \times \hat{\mathbf{x}}(t) < 0 \wedge |\hat{\mathbf{x}}(t)| > R$.

The Fig. 4 illustrates the following proposition, which is proven in the Appendix C.

Proposition 3 (AO-shape): The AO_τ is locally convex on its left boundary, iff the initial course is left-passing or pre-colliding, or it is locally concave there iff it is right-passing or post-colliding. And the analogous statement interchanging the words "left" and "right" holds as well.

B. Connection to Acceleration Velocity Obstacles

The family of relative trajectories $\mathbf{x}(t; \mathbf{v})$ underlying AVO [7] results from proportional velocity control with some gain $1/\delta > 0$ and setpoint $\mathbf{v} = const$, i.e. the motion satisfies

$$\ddot{\mathbf{x}} = (\mathbf{v} - \dot{\mathbf{x}})/\delta = \mathbf{a} - \dot{\mathbf{x}}/\delta \tag{9}$$

with $\mathbf{a} := \mathbf{v}/\delta$. When $\delta \to \infty$ and $|\mathbf{v}| \to \infty$ while maintaining a given value of $\mathbf{a}$, (9) approaches the motion model underlying AO, namely $\ddot{\mathbf{x}} = \mathbf{a}$. Indeed, it holds

$$\lim_{\delta \to \infty} AVO_\tau(\delta)/\delta \to AO_\tau \tag{10}$$

in the following sense. Denoting the AVO's center and radius functions by $\tilde{\mathbf{c}}$ and $\tilde{r}$, respectively, it holds that $\tilde{\mathbf{c}}(t; \delta)/\delta \to \mathbf{c}(t)$ and $\tilde{r}(t; \delta)/\delta \to r(t)$ as $\delta \to \infty$, for any fixed $t > 0$. The proof is given in the Appendix D.

III. Method

The technique we propose for a robot's navigation between multiple agents uses the AO and the theoretical results from the previous Section II.

A. Construction Scheme for AO-Constraints

From the AO_τ between the robot and a given obstacle, a linear constraint is constructed for the robot's acceleration. Let $H(\mathbf{n}, b) := \{\mathbf{z} \,|\, \mathbf{n}^T \mathbf{z} \leq b\}$ denote the closed halfplane with the outwards normal $\mathbf{n}$ and its boundary's offset b from the origin (along $\mathbf{n}$). For shorter notation, let $\tilde{\mathbf{x}} := \hat{\mathbf{x}}(\tilde{\tau})$. Given the parameters defining an AO_τ, the Algorithm 1 constructs a halfplane H which covers the AO_τ and whose boundary touches its cap $\mathcal{C}$, as illustrated by the Fig. 4 for various AO_τ.

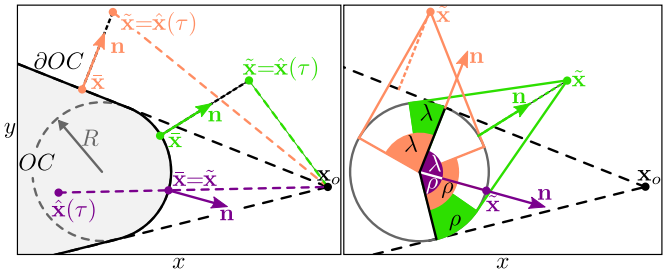

Fig. 5. Left: The Algorithm 1 projects the point $\tilde{\mathbf{x}}$ on the boundary ∂OC of the occlusion cone OC for the collider of radius R and the relative position $\mathbf{x}_o$. There at $\bar{\mathbf{x}}$, the surface normal $\mathbf{n}$ is extracted (shown for three $\tilde{\mathbf{x}}$ in purple, green, orange). The point $\tilde{\mathbf{x}}$ is the halftime prediction at the time horizon $\hat{\mathbf{x}}(\tau)$ if the latter is outside OC (green, orange cases), else $\tilde{\mathbf{x}}$ is at the intersection $\overline{\mathbf{x}_o\hat{\mathbf{x}}(\tau)} \cap \partial OC$ (purple case). Right: the AO_τ's left and right local boundaries' normals are constructed by drawing tangents to the circle and through $\hat{\mathbf{x}}(t)$ as t varies over $(0, \tilde{\tau}]$, and their resulting orientations' respective intervals are shown and labeled by λ and ρ, respectively.

Algorithm 1: Conservative Approximation of AO_τ.

Input: $\mathbf{x}_o$, $\mathbf{v}_o$, R
Output: $H(\mathbf{n}, b) \supset AO_\tau(\mathbf{x}_o, \mathbf{v}_o, R)$
1: $OC \leftarrow$ occlusion cone $OC(\mathbf{x}_o, R)$
2: $\bar{\mathbf{x}} \leftarrow \tilde{\mathbf{x}}$'s orthogonal projection on ∂OC
3: $\mathbf{n} \leftarrow OC$'s outwards normal at $\bar{\mathbf{x}}$
4: $b \leftarrow \mathbf{n}^T\mathbf{c}(\tilde{\tau}) + r(\tilde{\tau})$
5: **return** $H(\mathbf{n}, b)$

The Fig. 5 illustrates the geometric constructions performed by the Algorithm 1. To explain its steps and why the resulting halfplane is always conservative, we first note that for any $\mathbf{n}$, choosing b as in Line 4 ensures that ∂H touches $D_{\tilde{\tau}}$. As the Fig. 5 indicates, the algorithm constructs $\mathbf{n}$ such that the left and right boundary's normals are to its left and right, respectively, i.e. $\mathbf{n} \times \mathbf{n}' > 0, \forall \mathbf{n}' \in N^\lambda$ and $\mathbf{n} \times \mathbf{n}' < 0, \forall \mathbf{n}' \in N^\rho$. Thus, ∂H can neither intersect B^λ nor B^ρ, leading to the following proposition.

Proposition 4 (Conservative Halfplane): The halfplane H constructed by the Algorithm 1 is a conservative approximation of the AO_τ, i.e. $H \supseteq AO_\tau$.

A more formal proof is given in the Appendix E.

As AO may cover an infinitely large radius around the origin, we impose an upper bound $b_{\max} >> a_{\max}$ on b, i.e. we actually compute the limited offset $\hat{b} := \min(b, b_{\max})$, where b is defined by the Algorithm 1. This step ensures that the resulting halfplane $\hat{H} := H(\mathbf{n}, \hat{b})$ can serve as a (soft) constraint in a numerical optimization and also, from a theoretical point of view, does not dominate entirely the optimization's solution (Section III-C). In this work, we assume the obstacle's acceleration to be zero, such that $\hat{H}$ can be treated as in the space of the robot's absolute acceleration.

B. Limits of Acceleration and Velocity

Assuming that the robot's acceleration and velocity are restricted to given feasible convex sets A and V, respectively, our approach represents them as well by linear constraints on the robot's acceleration. This work sets $A = D(\mathbf{0}, a_{\max})$ and $V = D(\mathbf{0}, v_{\max})$, for simplicity, with $a_{\max} = 2$ ms^{-2} and $v_{\max} = 1.7$ m/s. Since V is in the space of velocity, it is transformed into the set of accelerations that keep the velocity within V over some time horizon $T_v > 0$, chosen as $T_v = 0.25$ s. Thus, let $\tilde{V} := (-\mathbf{v}_1(0) \oplus V)/T_v$, where $\mathbf{v}_1(0)$ is the robot's current velocity and $\oplus$ denotes Minkowski addition. Then, A and $\tilde{V}$ are under-approximated by the convex polygons $\mathcal{A} \subseteq A$ and $\mathcal{V} \subseteq \tilde{V}$, respectively. In this work, we define both approximations as the intersection of 16 respective halfplanes.

C. Command Optimization

Denoting the halfplane's parameters computed for the i-th obstacle by $\mathbf{n}_i, \hat{b}_i$, we combine these constraints from M obstacles with the objective of applying a given nominal acceleration $\bar{\mathbf{a}}_1$ in the quadratic program

$$\mathbf{a}_1^* := \arg\min_{\mathbf{a}} |\mathbf{a} - \bar{\mathbf{a}}_1|^2$$
$$\text{s.t. } \mathbf{n}_i^T\mathbf{a} \geq \hat{b}_i, i = 1, \ldots, M$$
$$\mathbf{a} \in \mathcal{A} \cap \mathcal{V}$$

whose solution $\mathbf{a}_1^*$ defines the robot's command. For the case that the above problem turns out to be infeasible, the control law is defined by the alternative problem to minimize the largest violation of an obstacle's constraint, as in prior work using VO [6]. This corresponds to the linear program

$$\mathbf{a}_1^*, \xi^* := \arg\min_{\mathbf{a}, \xi} \xi$$
$$\text{s.t. } \mathbf{n}_i^T\mathbf{a} \geq \hat{b}_i - \xi, i = 1, \ldots, M$$
$$\mathbf{a} \in \mathcal{A} \cap \mathcal{V}$$

whose feasibility is that of $\mathcal{A} \cap \mathcal{V}$. If it is infeasible, the robot must be moving with a velocity outside $\mathcal{V}$, which may happen in practice. In the infeasible case, the command is chosen as $\mathbf{a}_1^* = -a_{\max}\mathbf{v}_1/|\mathbf{v}_1|$ (opposed to the current velocity).

IV. Experiments

The next Section IV-A compares AO with AVO. Robots' navigation using AO and the SFM in bi-directional crowd flow simulations is evaluated in the Section IV-B. We provide videos of the crowd simulations in the supplementary material.

A. Comparison With AVO

In this experiment, the robot approaches a flat wall and brakes to avoid a collision. Since the obstacle is conceptually equal to a circle with infinite radius, the corresponding AVO and AO are halfplanes and one can directly interpret them as a linear constraint, which we then impose on the robot's motion. The largest absolute acceleration which the robot applies when braking in front of an obstacle is smaller for AO than for AVO with any finite relaxation time δ, as the Fig. 6 illustrates.

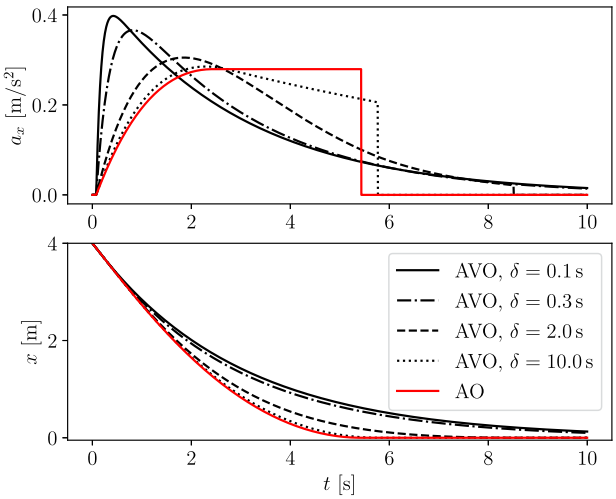

Fig. 6. A robot's braking acceleration a_x (top) and position x (bottom) over time are shown as it perpendicularly approaches a flat wall and avoids a collision (at $x = 0$) using AVO (with different relaxation times δ) or AO.

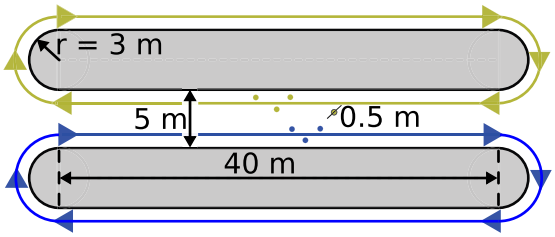

Fig. 7. The crowd forms two streams (blue and yellow) through a corridor.

B. Crowd–Robot Interaction in a Corridor

In the simulations, the robot travels in a corridor amidst two streams of pedestrians which move in mutually opposite directions (cf. Fig. 7) and are governed by the Social Force model (SFM) for pedestrian dynamics [10].

1) The Social Force Model (SFM): The SFM describes a pedestrian as a body with position $\mathbf{x}_i$ and velocity $\mathbf{v}_i$. Its acceleration is described as the sum of a driving force $\mathbf{f}_i$ towards the preferred velocity and repelling forces $\mathbf{f}_{i,j}, \tilde{\mathbf{f}}_{i,k}$ due to other pedestrians and walls, respectively. The driving force is defined as

$$\mathbf{f}_i := (\mathbf{v}_{des,i} - \mathbf{v}_i)/\gamma, \tag{11}$$

where $\mathbf{v}_{des,i}$ denotes the desired velocity and γ is the relaxation time. We denote by $\mathbf{e}_{i,j}$ the unit vector pointing from the j-th to the i-th pedestrian and by $d_{i,j}$ the distance between them (minus their radii). The force due to other pedestrians comprises long-range interactions with strength A_1 and range B_1 and short-range (physical) interactions with strength A_2 and range B_2 according to

$$\mathbf{f}_{i,j} = \mathbf{e}_{i,j}\left(A_1 e^{-d_{i,j}/B_1} w(\varphi_{i,j}) + A_2 e^{-d_{i,j}/B_2}\right), \tag{12}$$

with $w(\varphi_{i,j}) := \lambda + (1-\lambda)(1+\cos\varphi_{i,j})/2$ and $\cos\varphi_{i,j} = -\mathbf{e}_{i,j}\cdot\mathbf{v}_i$, where $\lambda \in [0,1]$ can be chosen below 1 to reduce interactions with pedestrians not in the viewing direction.

Similarly for walls, we denote by $\tilde{\mathbf{e}}_{i,k}$ the unit vector pointing from the k-th wall's nearest point to the i-th pedestrian and by $\tilde{d}_{i,k}$ the distance between them (minus the pedestrian's radius). The interaction force due to walls is defined as

$$\tilde{\mathbf{f}}_{i,k} = \tilde{\mathbf{e}}_{i,k} A e^{-\tilde{d}_{i,k}/B}. \tag{13}$$

with A and B specifying the repulsion's strength and range, respectively. Thus the i-th pedestrian's acceleration is given by

$$\ddot{\mathbf{x}}_i = \mathbf{f}_i + \sum_{j\neq i} \mathbf{f}_{i,j} + \sum_k \tilde{\mathbf{f}}_{i,k}. \tag{14}$$

In our simulations, we set the SFM parameters as [10], [14] to $\gamma = 1$ m/s, $A_1 = 0.42$ m/s^2, $B_1 = 1.65$ m, $A_2 = 3$ m/s^2, $B_2 = 0.2$ m, $\lambda = 0.75$, $A = 5$ m/s^2, $B = 0.2$ m.

2) Control of the Robot: For controlling the robot, we compare the method using the Acceleration Obstacle (AO) as defined in the previous Section III to two alternative methods. The first alternative applies the SFM to determine the robot's acceleration in the same way as for pedestrians. The second alternative combines the SFM and AO by computing the robot's nominal acceleration $\bar{\mathbf{a}}_1$ from the SFM and executing the method of AO to determine the actual acceleration $\mathbf{a}_1^*$ taking into account constraints due to pedestrians. We abbreviate the three methods for controlling the robot as AO, SF, and SF-AO, respectively. For AO, the nominal acceleration $\bar{\mathbf{a}}_1$ is computed according to (11).

3) Experimental Protocol: To obtain diverse states of the crowd in the corridor for initializing the experiments, we run a preliminary simulation of a system comprising 200 pedestrians (100 per direction) for a long duration. Starting from two separated streams (cf. Fig. 7), the system's state becomes less ordered after two minutes (in simulation), when we start to periodically take a snapshot of the system's state, with period $\Delta t = 20$ s, until a set of K states is obtained ($K = 48$). Due to chaotic fluctuations and spontaneous congestion, the crowd's density in the corridor varies across snapshots (from 0.28 to 0.5 persons per square meter).

In each snapshot, one particular pedestrian is chosen to be replaced by the robot, whereas the others serve to initialize the crowd in the actual experiments. For each snapshot, we carry out one simulation of duration Δt for each method to control the robot and for three different preferred speeds for the robot, namely 1.1, 1.3, and 1.5 m/s. A radius of 0.25 m is assumed for both the robot and pedestrians. Each pedestrian's preferred speed is constant throughout all experiments and sampled from the normal distribution with mean 1.3 and standard deviation 0.3 m/s. For AO and SF-AO, we set the time horizon to $\tau = 1$ s.

4) Metrics: We compute the following metrics by considering only the time span when the robot is inside the corridor.

The robot's efficiency is quantified in two ways. Firstly, the metric v_r is defined as the ratio of its average velocity in its preferred direction over its preferred speed [11]. Secondly, the metric p_r is defined as the ratio of its change in position in its preferred direction over its path length. Thus, p_r measures the path's efficiency independent from the velocity. The metrics v_c and p_c measure the analogous quantities' averages over pedestrians' trajectories in the corridor.

TABLE I
RESULTS OF SIMULATED BI-DIRECTIONAL CROWD FLOW IN A CORRIDOR INCLUDING A ROBOT THAT USES SF, AO, OR SF-AO

	v_r [-]	v_c [-]	p_r [-]	p_c [-]	L [-]	I [m/s^2]	C [-]	NM [-]
robot's preferred speed = 1.1 m/s								
SF	0.80 ±0.24	0.73 ±0.14	0.92 ±0.13	0.919 ±0.059	4.1 ±1.8	0.008 ±0.011	30	64
AO	**0.87***±0.16	**0.74***±0.13	**0.98***±0.03	**0.921***±0.056	3.7*±1.9	**0.007** ±0.009	2	89*
SF-AO	0.76*±0.28	0.73*±0.14	0.88*±0.31	0.918*±0.060	**4.1***±1.8	0.008 ±0.011	**1**	**36***
robot's preferred speed = 1.3 m/s								
SF	0.72 ±0.19	0.73 ±0.14	0.93 ±0.10	0.918 ±0.059	4.1 ±1.7	0.008 ±0.009	32	55
AO	**0.85***±0.18	**0.74***±0.13	**0.98***±0.03	**0.920** ±0.057	3.6*±1.8	**0.007***±0.008	3	98*
SF-AO	0.67*±0.25	0.73*±0.14	0.87*±0.30	0.919 ±0.060	**4.0***±1.7	0.009*±0.012	**2**	**50***
robot's preferred speed = 1.5 m/s								
SF	0.65 ±0.19	0.73 ±0.14	0.92 ±0.13	0.918 ±0.060	3.9 ±1.9	0.009 ±0.011	36	67
AO	**0.83***±0.19	**0.74** ±0.13	**0.99***±0.03	0.919 ±0.057	3.4*±1.8	**0.006***±0.009	4	99*
SF-AO	0.62*±0.23	0.73 ±0.14	0.91*±0.17	**0.920** ±0.057	**3.9***±1.9	0.009*±0.014	**1**	**54***

The robot's integration in lanes is measured by the metric L, which denotes the temporal average of the number of pedestrians around the robot (i.e. 5 m close) that have the same preferred direction of motion and differ in the transversal coordinate (in the direction orthogonal to the walls) by at most 0.5 m from the robot. The metric I measures for pedestrians heading the other way than the robot the average acceleration induced by the robot via (12) in the component opposed to their preferred direction.

When two agents' distance falls below the sum of their radii, a collision is counted. A near miss is defined similarly as the event that the distance between two agents becomes lower than the sum of their radii plus 0.1 m but no collision occurs while this condition is present. The metrics C and NM count pedestrian-robot collisions and near misses, respectively, only considering events in the corridor.

5) Results: Comparing the robot's control methods SF, AO, and SF-AO, the Table I gives separate results for the robot's three different preferred velocities. It gives the mean and standard deviation over the K executions for the velocity and path efficiency metrics, and the sum over the K executions for the collision and near miss metrics. Asterisks (*) indicate that a t-test rejects the null-hypothesis that the expected value of the difference between the respective metric of AO and SF-AO is equal to zero (p-value < 0.05). In this case, the difference is considered significant. Values in bold indicate the best performance.

When the robot uses AO, both the robot and the crowd move more efficiently in their preferred direction (and also faster), as the values of v_r, v_c, p_r, and p_c show. On the other hand, the method SF-AO leads to the smallest number of collisions and near misses between the robot and the crowd. The robot's tendency to integrate itself in lanes as measured by L is higher with SF-AO than with AO. However, its interaction intensity with the opposite stream as measured by I is lower with AO than with SF-AO. With SF, the robot's efficiency's mean value and the number of near misses are between SF-AO and AO. The largest number of collisions is reported for SF.

6) Discussion: The robot progresses faster with AO because it can use any free space to navigate, in particular the corridor's middle, which is often free because pedestrians repell each other on a long range and therefore tend to stay close to the walls (cf. Fig. 8). With AO in contrast, the robot tends to come arbitrarily close to pedestrians, which is reflected by the large number of near misses. Pedestrians tend to restore the distance since the robot repells them like a pedestrian. Therefore, the robot also makes pedestrians progress faster by pushing them forward when approaching from behind. This happens frequently because the crowd tends to form lanes and the robot is initialized in place of a pedestrian and thus often in a lane.

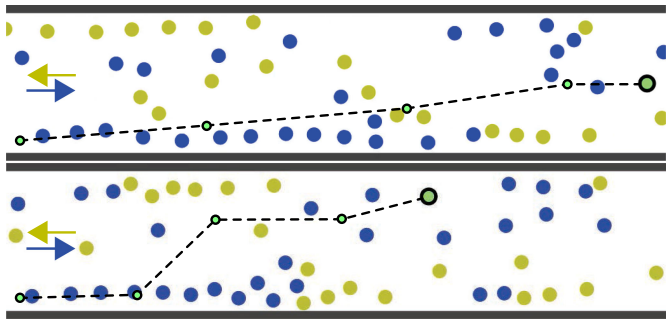

Fig. 8. Both snapshots show a simulation from the same initial condition once with AO (top) and SF-AO (bottom). Pedestrians (blue/yellow) tend to form lanes close to the walls due to mutual repulsion. The robot (large black-green circle) has the same tendency with SF-AO, whereas it can navigate in the free middle between lanes when using AO. Its path is shown by connecting four past waypoints (dashed line/small black-green circles).

With SF-AO, the robot maintains a similar distance to pedestrians as they do among each other, as indicated by the smaller number of near misses than with AO. The distance margin leaves the robot more time to react to pedestrians' changing velocities, which explains why fewer collisions occur than with AO. Since a higher number of near misses implies a higher (actual and perceived) risk of collisions, navigation with AO is riskier but more efficient than with SF-AO, while only very few actual collisions occur, comparing to SF. Thus, the two methods AO and SF-AO represent different priorites on the safety–efficiency spectrum, which has been described in prior work [15] as trade-off inherent to navigation in a crowd.

While related work often uses efficiency to quantify lane formation [11], [16], the robot in our simulations can achieve higher efficiency outside lanes. The fact that AO achieves higher values of v_r, v_c, p_r, and p_c while exhibiting lower values of L and I than SF-AO can be explained as follows. The robot with AO may leave lanes earlier than with SF-AO and avoid the opposite stream successfully by exploiting narrow gaps without decreasing the opposite stream's efficiency. Thus, the robot's

superior performance at avoiding oppositely headed pedestrians by AO (also reflected by low interaction intensity I) seems to over-compensate being less often in lanes. Considering that the crowd's efficiency is positively affected by AO (considering v_c, p_c), the robot does not seem to obstruct lane formation, even when not participating in it. The efficiency metrics exhibit larger standard deviations with SF-AO and SF, since the robot is repelled by the crowd and thus more sensitive to its fluctuating density.

V. Conclusion

In this letter, we have studied Acceleration Obstacles (AO) in the context of robotic navigation in human crowds, focusing particularly on bi-directional flow in corridors. We have described the AO geometrically and analyzed how its shape depends on parameters. We have related the Acceleration Velocity Obstacle (AVO) to the AO via a limit case, which requires the least braking deceleration. A method has been proposed for a robot's navigation using AO via a novel algorithm which exploits our geometric analysis of AO to compute conservative linear approximations of AO in closed form. For the experimental evaluation, we have used the Social Force Model (SFM) to simulate crowds which interact with a robot. Applying our method, the robot progresses faster and undergoes very few collisions in comparison to pedestrians. Since many near misses still indicate a risk of collision, future work could address this issue e.g. by adaptive distance margins or objective functions that include social norms. The combination of the SFM and the AO has been evaluated as an alternative robotic controller, which was found to be significantly less efficient. Furthermore, we have shown that the robot could achieve higher performance when being less often in lanes.

Appendix

A. Proof of Proposition 1 (AO-Normals)

With $f(\mathbf{z},t) := |\mathbf{z}-\mathbf{c}(t)|^2 - r^2(t)$, the intersection of infinitesimally close circles (5) is expressed by the two equations $f(\mathbf{z},t)=0$ and $f(\mathbf{z},t+\mathrm{d}t)=0$ in the unknown $\mathbf{z}\in\mathbb{R}^2$. Subtracting the first from the second equation and dividing by $\mathrm{d}t$ yields $\partial f(\mathbf{z},t)/\partial t = 0$ as $\mathrm{d}t\to 0$, or

$$0 = -\frac{1}{2r(t)}\frac{\partial f(\mathbf{z},t)}{\partial t} = \frac{(\mathbf{z}-\mathbf{c}(t))^T\dot{\mathbf{c}}}{r(t)} + \dot{r}. \tag{15}$$

With $\mathbf{n}_t = (\mathbf{z}-\mathbf{c})/r$ according to (6), one has equivalently

$$\mathbf{n}_t^T\dot{\mathbf{c}} + \dot{r} = 0, \quad |\mathbf{n}_t| = 1. \tag{16}$$

Computing derivatives from (3), one obtains

$$\mathbf{n}_t^T\frac{4}{t^3}(\mathbf{x}_o+\mathbf{v}_o t/2) - \frac{4R}{t^3} = 0$$
$$\mathbf{n}_t^T(\mathbf{x}_o+\mathbf{v}_o t/2) - R = 0, \quad |\mathbf{n}_t| = 1.$$

Thus, the proof is complete. In [13], the condition given for a canal's boundary to exist is $|\dot{\mathbf{c}}| \geq |\dot{r}|$, which corresponds to (16) admitting any solution.

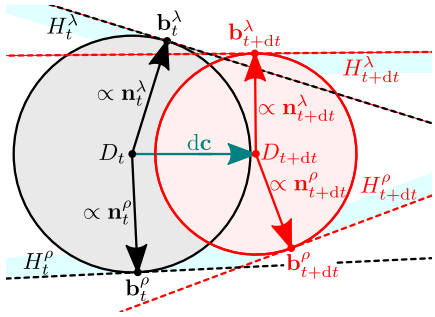

Fig. 9. For a given t and small increment dt, an AO_τ's disks D_t and $D_{t+\mathrm{d}t}$ are shown with their left and right local boundaries $\mathbf{b}^\lambda$, $\mathbf{b}^\rho$, the associated normals $\mathbf{n}^\lambda$, $\mathbf{n}^\rho$, and the tangent halfplanes H^λ, H^ρ, respectively. One side's boundary is locally convex (concave) when each disk's tangent halfplane does (not) contain the other disk's tangent point as $\mathrm{dt}\to 0$.

B. Proof of Proposition 2 (AO-Reduction)

In the non-trivial case that $\tilde{\tau}\neq\tau$, the line segment from $\mathbf{x}_o$ to $\hat{\mathbf{x}}(\tau)$ intersects the disk $D(\mathbf{0},R)$ at the point $\hat{\mathbf{x}}(\tilde{\tau})$. According to the Proposition 1, at every $t<\tilde{\tau}$, there are two distinct normals and boundary points, whereas at $t=\tilde{\tau}$, there is only one normal and boundary point. Since (7) is continuous in t, it follows that the local boundary forms two distinct branches for $t<\tilde{\tau}$ which meet when $t=\tilde{\tau}$. Hence, it remains to show that the local boundary over $(0,\tilde{\tau}]$ delimits a shape which contains the canal for any $t'>\tilde{\tau}$. By the Definition 2, the local boundary point for any time t with a given normal $\mathbf{n}_t$ is

$$\mathbf{b}_t = \mathbf{c}(t) + \mathbf{n}_t r(t) = 2\left(R\,\mathbf{n}_t - \mathbf{x}_o - \mathbf{v}_o t\right)/t^2.$$

Let H_t denote the halfplane with normal $\mathbf{n}_t$ whose boundary ∂H_t touches the local boundary at $\mathbf{b}_t$, calculated as

$$\begin{aligned} H_t &= \left\{\mathbf{a}|\mathbf{a}^T\mathbf{n}_t \leq \mathbf{n}_t^T\mathbf{b}_t\right\} \\ &= \left\{\mathbf{a}|\mathbf{a}^T\mathbf{n}_t \leq -\mathbf{n}_t^T\mathbf{v}_o/t\right\} \end{aligned}$$

Thus, for some (different) time t', it holds $D_{t'}\subset H_t$ iff

$$\begin{aligned} \mathbf{c}(t')^T\mathbf{n}_t + r(t') \leq -\mathbf{n}_t^T\mathbf{v}_o/t \iff \\ R - \hat{\mathbf{x}}(t)^T\mathbf{n}_t + \mathbf{n}_t^T\mathbf{v}_o\Delta t^2/(2t) \leq 0 \iff \\ \mathbf{n}_t^T\mathbf{v}_o\Delta t^2/(2t) \leq 0 \end{aligned}$$

with $\Delta t := t'-t$, where the last step uses (7). It is easy to see that for any $t\in(0,\tilde{\tau}]$, it holds $\mathbf{n}_t^T\mathbf{v}_o\leq 0$ (cf. Fig. 3(b)). Hence, the condition is true for all t', which means that H_t contains the entire AO_τ. As this holds for every point on the local boundary with $t<\tilde{\tau}$, the AO_τ cannot intersect this boundary, which proves that the $AO_{\tilde{\tau}}$ contains subsequent disks, i.e. $AO_\tau = AO_{\tilde{\tau}}$.

C. Proof of Proposition 3 (AO-Shape)

For any time t and a small increment dt, we consider the two disks D_t and $D_{t+\mathrm{d}t}$ (cf. Fig. 9). As $\mathrm{d}t\to 0$, we consider for one local boundary (left or right) how $\mathbf{b}_t$ and $\mathbf{b}_{t+\mathrm{d}t}$ converge, i.e. their constellation with respect to each other's tangent halfplane H_t and $H_{t+\mathrm{d}t}$. If $\mathbf{b}_t\notin H_{t+\mathrm{d}t}$ and $\mathbf{b}_{t+\mathrm{d}t}\notin H_t$ as for the left boundary in the Fig. 9, they describe a locally concave boundary.

Else if $\mathbf{b}_t \in H_{t+\mathrm{d}t}$ and $\mathbf{b}_{t+\mathrm{d}t} \in H_t$, a locally convex boundary is described, as for the right boundary in the Fig. 9. The other two possible constellations (mixing $\in$ and $\notin$) are equivalent to the point $\mathbf{b}_t$ being contained within nearby disks' interiors and thus not contributing to the AO's boundary.

One finds (cf. Fig. 3) that both the left and right normal rotates monotonically with t on $(0, \tilde{\tau}]$. From the aforementioned constellations, the one describing a concave boundary is compatible with the normal rotating counter-clockwise, if it is the left boundary, or clockwise, if it is the right boundary. And the constellation describing a convex boundary is compatible with the normal rotating clockwise, if it is the left boundary, or counter-clockwise, if it is the right boundary. Both constellations are incompatible with the other sense of monotonic rotation in each case. Thus, the left boundary is convex iff its normals rotate clockwise, and it is concave iff its normals rotate counter-clockwise, whereas the right boundary is convex iff its normals rotate counter-clockwise, and it is concave iff its normals rotate clockwise.

Looking at the Fig. 3, one can verify quickly that the direction of rotation for both the left and the right normals is counter-clockwise if $\hat{\mathbf{x}}$ passes on the right of the disk $D(\mathbf{0}, R)$, whereas it is clockwise if passing on the other side. On the other hand, when on a pre-colliding course, the left and right normals rotate clockwise and counter-clockwise, respectively. When on a post-colliding course, the opposite holds. Combining these observations with the above considerations, the Proposition 3 follows.

D. Proof of AVO Converging to AO

AVO's center and radius functions [7] are respectively

$$\tilde{\mathbf{c}}(t) = \frac{\delta\left(e^{-t/\delta}\mathbf{v}_o - \mathbf{x}_o\right)}{t + \delta\left(e^{-t/\delta} - 1\right)}, \tilde{r}(t) = \frac{R}{t + \delta\left(e^{-t/\delta} - 1\right)}.$$

One can then obtain the expressions

$$\frac{\tilde{\mathbf{c}}(t)}{\delta} = -\frac{\mathbf{x}_o + \mathbf{v}_o t}{g(\delta)} + \frac{\mathbf{v}_o}{\delta}, \frac{\tilde{r}(t)}{\delta} = \frac{R}{g(\delta)},$$

with $g(\delta) := \delta(t + \delta\left(e^{-t/\delta} - 1\right))$. Their limits for $\delta \to \infty$ are determined by g's limit, which can be calculated as $\lim_{\delta\to\infty} g(\delta) = t^2/2$, e.g. via the exponential's power series expansion. Comparing with (3), it follows that

$$\lim_{\delta\to\infty} \frac{\tilde{\mathbf{c}}(t)}{\delta} = -\frac{\mathbf{x}_o + \mathbf{v}_o t}{t^2/2} = \mathbf{c}(t), \lim_{\delta\to\infty} \frac{\tilde{r}(t)}{\delta} = \frac{2R}{t^2} = r(t).$$

E. Proof of the Proposition 4 (Conservative Halfplane)

To prove the proposition, we show that the halfplane H also admits the interpretation as the set of accelerations that would cause within the time horizon a collision not with the actual combined collider $D(\mathbf{0}, R)$ (in Fig. 5) but with the halfplane $\bar{H} \supset D(\mathbf{0}, R)$ whose boundary touches $D(\mathbf{0}, R)$ at $R\mathbf{n}$. To show this, let $\overline{AO}_\tau(\mathbf{n}) := \{\mathbf{a} | \exists t \in [0, \tau] : \mathbf{x}(t; \mathbf{a}) \in H(\mathbf{n}, R)\}$ define the acceleration obstacle for halfplanes. It contains all accelerations that would make the two bodies collide within the time horizon τ under the motion model (1) if their shapes were halfplanes whose boundaries touch the original bounding circles and are orthogonal to $\mathbf{n}$. One can show that $\overline{AO}_\tau(\mathbf{n}) = H(\mathbf{n}, a)$, where $a := \max_{t\in[0,\tau]} f(t)$ with $f(t) := 2(R - \mathbf{n}^T(\mathbf{x}_o + \mathbf{v}_o t))/t^2$. If there is $t^* > 0$ solving $f'(t) = 0 \iff R = \mathbf{n}^T\hat{\mathbf{x}}(t)$, then $f(t^*)$ is a global maximum on $(0, \infty)$, because $f'(t) > 0\,\forall t \in (0, t^*)$ and $f'(t) < 0\,\forall t \in (t^*, \infty)$. Else, $f'(t) > 0\,\forall t \in (0, \infty)$. Therefore, if there is $t^* > 0$, $a = f(\min\{t^*, \tau\})$, else $a = f(\tau)$. It can be seen now that $a = f(\tilde{\tau})$ when the normal $\mathbf{n}$ is chosen according to the Algorithm 1. There, the Line 4 can also be expressed as $b = f(\tilde{\tau})$. Thus, it holds $a = b$, which proves that aforementioned interpretation is valid, i.e. both approaches lead to the same halfplane in acceleration space, which is conservative as $D(\mathbf{0}, R) \subset \bar{H}$.

REFERENCES

[1] M. Pfeiffer, U. Schwesinger, H. Sommer, E. Galceran, and R. Siegwart, "Predicting actions to act predictably: Cooperative partial motion planning with maximum entropy models," in *Proc. IEEE/RSJ Int. Conf. Intell. Robots Syst.*, 2016, pp. 2096–2101.

[2] A. Vemula, K. Muelling, and J. Oh, "Social attention: Modeling attention in human crowds," in *Proc. IEEE Int. Conf. Robot. Automat.*, 2018, pp. 4601–4607.

[3] S. Bouraine, T. Fraichard, and H. Salhi, "Provably safe navigation for mobile robots with limited field-of-views in dynamic environments," *Auton. Robots*, vol. 32, no. 3, pp. 267–283, Nov. 2012.

[4] S. B. Liu, H. Roehm, C. Heinzemann, I. Lütkebohle, J. Oehlerking, and M. Althoff, "Provably safe motion of mobile robots in human environments," in *Proc. IEEE/RSJ Int. Conf. Intell. Robots Syst.*, 2017, pp. 1351–1357.

[5] P. Fiorini and Z. Shiller, "Motion planning in dynamic environments using velocity obstacles," *Int. J. Robot. Res.*, vol. 17, no. 7, pp. 760–772, 1998. [Online]. Available: https://doi.org/10.1177/027836499801700706

[6] J. van den Berg, S. J. Guy, M. Lin, and D. Manocha, "Reciprocal n-body collision avoidance," in *Proc. Robot. Res.*, Berlin, Heidelberg, 2011, pp. 3–19.

[7] J. van den Berg, J. Snape, S. J. Guy, and D. Manocha, "Reciprocal collision avoidance with acceleration-velocity obstacles," in *Proc. IEEE Int. Conf. Robot. Automat.*, 2011, pp. 3475–3482.

[8] D. Bareiss and J. van den Berg, "Generalized reciprocal collision avoidance," *Int. J. Robot. Res.*, vol. 34, no. 12, pp. 1501–1514, 2015. [Online]. Available: https://doi.org/10.1177/0278364915576234

[9] B. Damas and J. Santos-Victor, "Avoiding moving obstacles: The forbidden velocity map," in *Proc. IEEE/RSJ Int. Conf. Intell. Robots Syst.*, 2009, pp. 4393–4398.

[10] D. Helbing, L. Buzna, A. Johansson, and T. Werner, "Self-organized pedestrian crowd dynamics: Experiments, simulations, and design solutions," *Transp. Sci.*, vol. 39, no. 1, pp. 1–24, 2005.

[11] D. Helbing and T. Vicsek, "Optimal self-organization," *New J. Phys.*, vol. 1, Aug. 1999, Art. no. 13. [Online]. Available: https://doi.org/10.1088/1367-2630/1/1/313

[12] J. van den Berg, S. Patil, J. Sewall, D. Manocha, and M. Lin, "Interactive navigation of multiple agents in crowded environments," in *Proc. Symp. Interactive 3D Graph. Games*, New York, NY, USA, 2008, pp. 139–147. [Online]. Available: https://doi.org/10.1145/1342250.1342272

[13] M. Peternell and H. Pottmann, "Computing rational parametrizations of canal surfaces," *J. Symbolic Comput.*, vol. 23, no. 2, pp. 255–266, 1997. [Online]. Available: https://www.sciencedirect.com/science/article/pii/S0747717196900875

[14] A. Johansson, D. Helbing, and P. K. Shukla, "Specification of the social force pedestrian model by evolutionary adjustment to video tracking data," *Adv. complex Syst.*, vol. 10, no. supp02, pp. 271–288, 2007.

[15] F. Grzeskowiak et al., "Crowd against the machine: A simulation-based benchmark tool to evaluate and compare robot capabilities to navigate a human crowd," in *Proc. IEEE Int. Conf. Robot. Automat.*, 2021, pp. 3879–3885.

[16] J. Kirkland and A. Maciejewski, "A simulation of attempts to influence crowd dynamics," in *Proc. IEEE Int. Conf. Syst., Man Cybern.*, 2003, pp. 4328–4333.